JOURNAL OF GEOPHYSICAL RESEARCH, VOL. 105, NO. B5, PAGES 11,171–11,183, MAY 10, 2000

Compensation of the Ontong Java Plateau by surface and subsurface loading

Garrett Ito

Department of Geology, University of California, Davis

Asahiko Taira

Ocean Research Institute, University of Tokyo, Tokyo

Abstract. Gravity data over Ontong Java Plateau reveal deep crustal structure supporting the plateau's topography. At long wavelengths (>500 km), new shipboard gravity and bathymetry profiles indicate local isostatic compensation. At intermediate wavelengths (250-500 km), however, Bouguer anomalies have large amplitudes, too high to be explained by models of Airy isostasy or volcanic loading on the surface of an elastic lithospheric plate. This finding is also evident in admittance functions, generated from maps of bathymetry and satellite-derived Bouguer anomalies, which show high values at intermediate wavelengths. In addition, coherence between two-dimensional Bouguer gravity and bathymetry spectrums decreases to zero, beginning at intermediate wavelengths. Two possible models can explain the high admittance and low coherence at intermediate wavelengths. The first model explains the high admittance by large-scale lithospheric folding and explains the low coherence by sedimentation and erosion that is uncorrelated with the igneous crustal structure. Lithospheric folding might result from tectonic compression imposed on Ontong Java by the Solomon arc and trench system. The second model involves a multiple-stage accretion history with surface magmatism on a thin elastic plate and magmatic underplating beneath a thick plate. The thick plate during underplating is required to explain the high admittance values at intermediate wavelengths, while decorrelation between underplating and the surface loaded magmas can explain the low coherence. The thick plate also suggests that the lithosphere cooled appreciably since the first magmatic stage and therefore magmatic underplating occurred at a significantly later time than the initial eruption. Calculations predict that the underplated material could comprise as much as 50% of the total crustal volume, suggesting that the later eruptive stage(s) may have been as, or more voluminous than, the first.

1. Introduction

The Cretaceous period was a time of intense global magmatism, during which many of Earth's largest igneous provinces erupted on the continents and ocean basins [e.g., *Larson*, 1991]. The Ontong Java Plateau (OJP) in the western Pacific (Plate 1a) is one such province and is likely the most voluminous igneous edifice on Earth [*Coffin and Eldholm*, 1993]. Frozen into the structure of Ontong Java's crust is a record of its accretion and deformation history. Improved constraints and analyses of this structure are therefore needed to better our understanding of the mantle and tectonic processes that shaped this giant oceanic plateau.

Gravity and bathymetry data are used widely to constrain crustal structure as well as compensation mechanisms of topography in both oceanic and continental settings. Gravity anomalies of oceanic volcanoes, for example, are sensitive to the elastic strength of the lithosphere upon which volcanoes were emplaced [*McKenzie and Bowin*, 1976; *Watts and Cochran*, 1974]. Elastic plate thickness (T_e) is a measure of elastic strength and, in oceanic settings, reflects the thermal age of lithosphere at the time of volcanic loading [e.g., *McNutt*, 1984; *Watts*, 1978; *Watts et al.*, 1980]. Elastic plate thickness can therefore be used to infer the proximity of a plateau to a mid-ocean ridge, as well as the relative timing between major magmatic events [*Goslin and Diament*, 1987; *McNutt et al.*, 1997; *Watts et al.*, 1980]. In addition, ratios and correlations between Fourier spectrums of gravity and bathymetry anomalies have been used to constrain elastic plate thickness, as well as the importance of surface, versus subsurface sources of topography [*Forsyth*, 1985; *Jin et al.*, 1994; *Louden and Forsyth*, 1982; *McNutt*, 1983; *Stephenson and Lambeck*, 1985; *Zuber et al.*, 1989]. In the context of oceanic plateaus we refer to a surface load as mass emplaced on top of the elastic lithosphere, such as sediments and volcanic crust, as well as changes in topography due to erosion. We refer to a subsurface load as any vertical force on the lithosphere other than a surface load. Subsurface loads may arise from anomalously low-density mantle [*Sandwell and Renkin*, 1988], magmatic underplating [*Caress et al.*, 1995; *Watts et al.*, 1985], as well as lithospheric deformation due to tectonic stresses [e.g., *Jin et al.*, 1994; *McAdoo and Sandwell*, 1985; *Zuber*, 1987].

To determine the structure and loading history of the Ontong Java Plateau, we analyze gravity and bathymetry anomalies using a number of different methods. First, we analyze newly obtained shipboard bathymetry and gravity profiles over two major constructs of OJP. We then incorporate other shipboard and gridded data to produce maps of bathymetry and Bouguer

Paper number 2000JB900036.
0148-0227/00/2000JB900036$09.00

gravity. From these maps we generate admittance and coherence functions and examine different loading histories that explain the observations. We will demonstrate that the structure of OJP was strongly influenced by subsurface loading, well after the initial emplacement of OJP. This finding has important implications for the tectonic and accretion history of the Ontong Java Plateau.

2. Shipboard Bathymetry and Gravity Profiles

2.1. Data and Observations

In this first analysis we focus on new bathymetry and gravity data obtained from Leg 2 of cruise KH98-1 (R/V *Hakuho-Maru*, Ocean Research Institute (ORI), University of Tokyo). Our survey tracks include two main transects: line 1, extending SW-NE over Ontong Java's Eastern Salient; and line 2, extending E-W from the Nauru Basin on to the northern or High Plateau (Plate 1a). Free-air gravity measurements were made every 60 s using the National Institute of Polar Research-ORI Surface Ship Gravimeter. Measurement errors were ≤3 mGal along individual survey lines, most of which were evident in high-frequency variations associated with navigation errors. These high-frequency signals were removed by applying a low-pass filter in the Fourier domain, which removed wavelengths <2-4 km. The bathymetry data were obtained from the center beam of the Hakuho-Maru SeaBeam system.

Bathymetry and free-air gravity profiles are shown in Figure 1. Both the Eastern Salient (Figure 1a) and the High Plateau rise 2-3 km above the Nauru Basin to the east of OJP. The Eastern Salient is an elongate feature ~300 km in width where we crossed it. Our ship track over the High Plateau (Figure 1b) crosses some of the shallowest and possibly thickest portions of OJP. Both of the free-air gravity profiles are dominated by short-wavelength variations (λ < 200 km) which correlate with variations in seafloor topography. The profiles show very small amplitude at long wavelengths (>500 km) even though the long-wavelength topography is greatest. The satellite-derived free-air gravity data of the region (Plate 1b [*Sandwell and Smith*, 1997]) also show dominant amplitudes at short and intermediate wavelengths, indicating that this general characteristic extends over the whole plateau.

To isolate the gravitational signal due to subsurface structure, we generated profiles of Bouguer gravity anomalies. In this calculation we first produced bathymetry maps of the surrounding region (Plate 1a) by combining our data with other shipboard (National Geophysical Data Center (NGDC)) and gridded (ETOPO5) bathymetry data. This was done by eliminating all ETOPO5 points within 5 min of any ship point and then gridding the combined data set at 1.5-min intervals using a continuous curvature algorithm [*Wessel and Smith*, 1995]. The original shipboard data contained 5178 crossover points with a mean and rms crossover error of 44 m and 109 m, respectively. We then computed the gravitational attraction of the seafloor-water interface by filtering the two-dimensional (2-D) Fourier transform of the bathymetry map [*Parker*, 1973]. Three terms in *Parker's* [1973] summation were used in calculating these topographic effects. This signal was then computed along the ship tracks by interpolating values from the grids adjacent to the ship track coordinates. We then subtracted these predicted profiles from the KH98-1 free-air gravity profiles to generate Bouguer gravity anomaly profiles. Upper crustal and water densities were assumed to be 2700 kg/m^3 [*Gladczenko et al.*, 1997] and 1000 kg/m^3, respectively. In addition to Bouguer anomalies along our ship profiles, we also generated a map of Bouguer anomaly (Plate 2a). This was done by removing the gravitational effects of seafloor topography from satellite-derived free-air gravity grids [*Sandwell and Smith*, 1997].

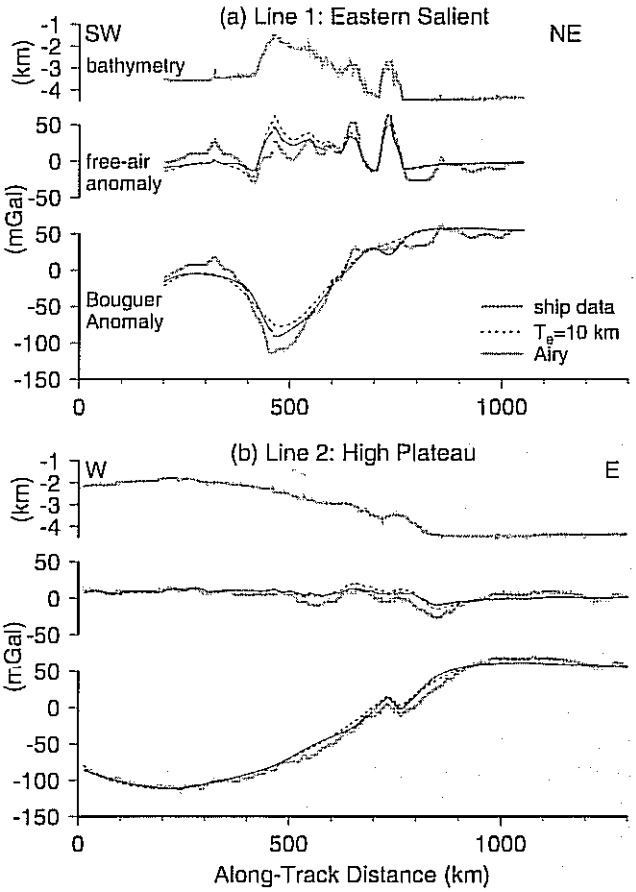

Figure 2. Observed admittance (equation (3), dots) for (a) the Eastern Salient and (b) the High Plateau. The wavelength of each point is the central wavelength within each wave number bin and error bars indicate standard deviations. Also shown are theoretical profiles (equation (2)) assuming Airy isostasy (gray) and surface loading of an elastic plate of thickness, T_e = 10 km (dashed). Coherence between Bouguer gravity and bathymetry maps (equation (4)) for (c) Eastern Salient and (d) High Plateau. The theoretical profiles for Airy isostasy (T_e = 0 km) and T_e = 10 km predict a coherence of 1.0 at all wavelengths.

The resulting Bouguer gravity anomalies along our ship tracks (Figure 1) show little variation at short wavelengths, thus indicating that topography is the dominant cause of the short-wavelength variations in free-air gravity. In contrast at longer wavelengths, Bouguer gravity anomalies are large and approximately mirror topography, with high-amplitude lows over topographic highs. Like our ship-derived profiles, the map of Bouguer anomaly is dominated by long- and intermediate-wavelength lows over the major edifices of OJP (Plate 2a). Because the Bouguer gravity anomaly is sensitive to undulations of the crust-mantle interface (Moho), an important source of these Bouguer lows is likely to be the thickened volcanic crust supporting the large-scale topography of OJP.

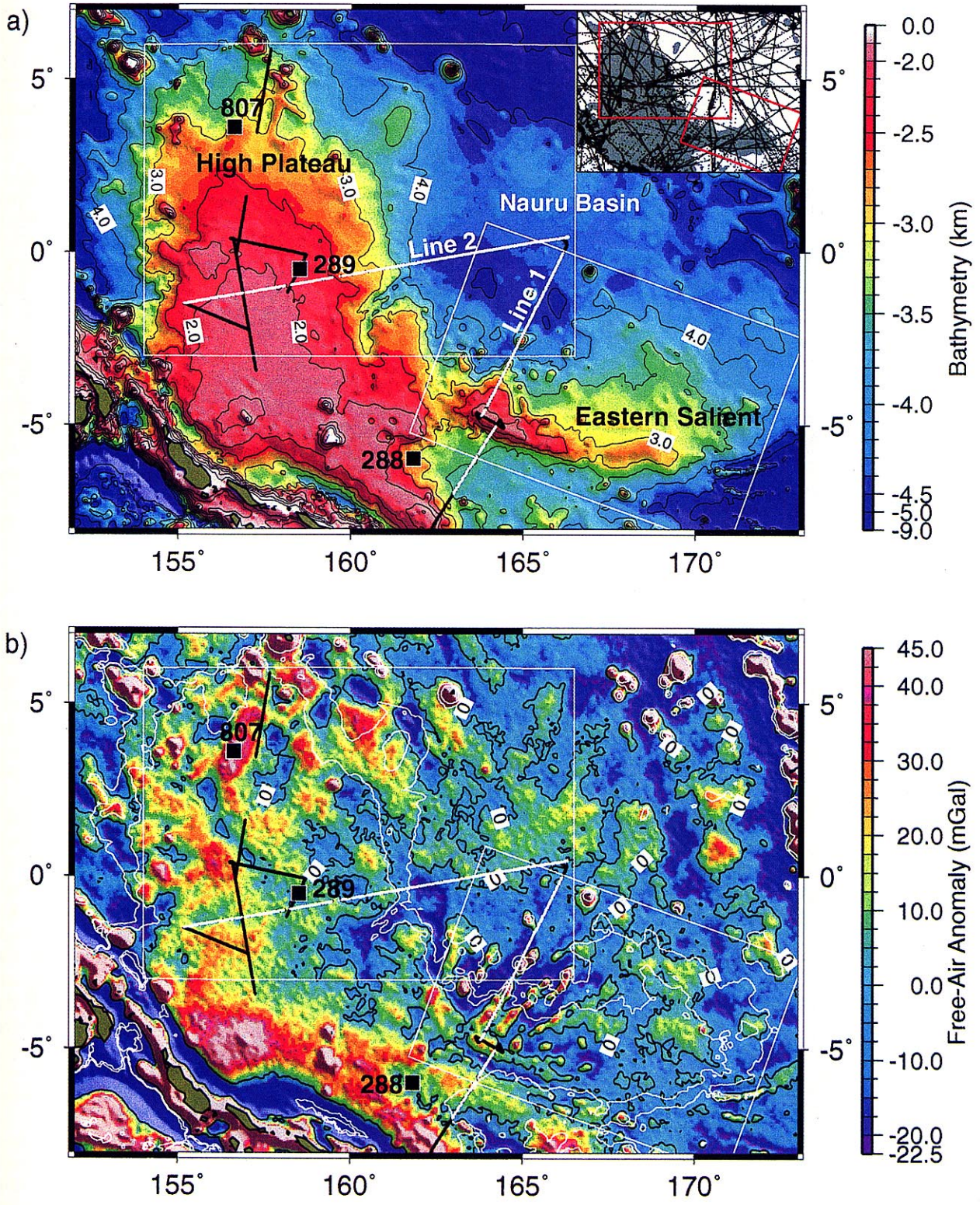

Plate 1. (a) Bathymetry map generated by combining cruise KH98-1 data (ship tracks shown), existing shipboard data from National Geophysical Data Center (NGDC) (points shown in inset, shading denotes depths <3.5 km) and gridded ETOPO5 data. Contour interval is 0.5 km. Gravity profiles are along lines 1 and 2 (white). White rectangles outline the subregions used in the admittance and coherence analysis. Ocean Drilling Program/Deep Sea Drilling Project (ODP/DSDP) drill sites used in subsidence analyses [*Ito and Clift*, 1998] are labeled. Illumination is from the NE in all plates. (b) Satellite-derived free-air gravity from *Sandwell and Smith* [1997]. The zero contour is shown in black, and the 3.5- and 4.0-km-depths are contoured in white. This and the other figures were generated using GMT [*Wessel and Smith*, 1995].

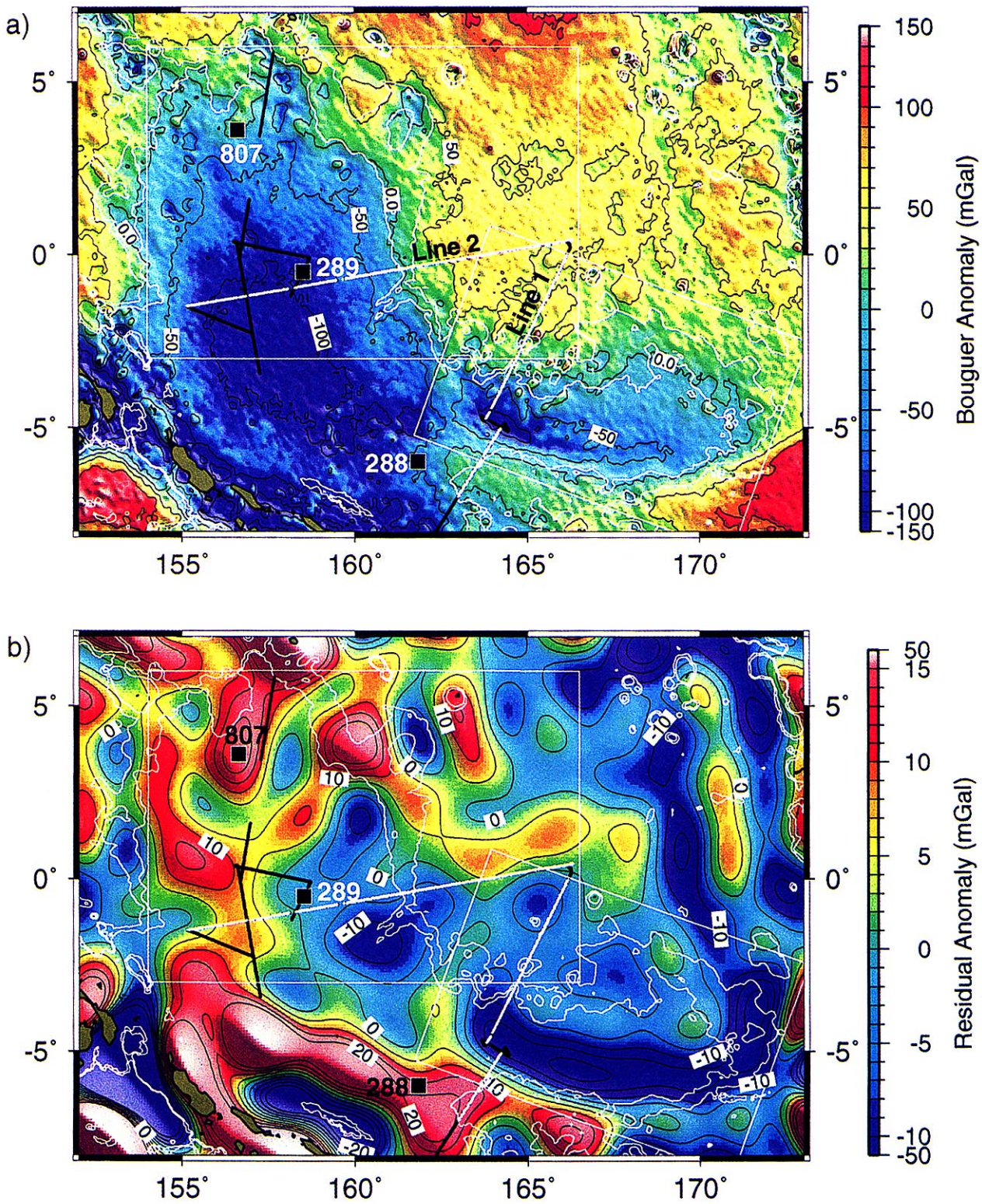

Plate 2. (a) Bouguer gravity map generated by removing topographic effects from the satellite-derived free-air gravity grid (Plate 1b). The mean value is subtracted. Contours at 50-mGal intervals are shown in black, and the 3.5- and 4.0-km depths are contoured in white. Only data contained in the white rectangles are used in producing observed admittance and coherence functions. (b) Residual anomaly is the observed Bouguer anomaly (Plate 2a) minus that predicted by Airy isostasy. Short wavelengths (λ) were removed by applying a low-pass filter beginning at $\lambda = 300$ km and tapering to zero at $\lambda = 200$ km. Contour interval (black) is 5 mGal.

2.2. Models of Surface Loading

To determine how topography of OJP is compensated, we first examine models in which volcanism loads the surface of an elastic lithospheric plate. As derived by *Dorman and Lewis* [1970], each Fourier component of Bouguer gravity $B(k)$ and topography $H(k)$ can be related by a linear transfer function, or admittance function, $Q(k)$:

$$B(k) = Q(k)\, H(k), \quad (1)$$

where $k = 2\pi/\lambda$ is the magnitude of the 2-D wave number k. To first order, the Bouguer anomaly is caused by undulations of the Moho. With this assumption the theoretical admittance function for surface loading of an elastic plate is [*Banks et al.*, 1977; *McKenzie and Bowin*, 1976]

$$Q(k) = -2\pi\rho_0 G \exp(-kz_c)/\xi, \quad (2)$$

where G is the gravitational constant, $z_c = 21.7$ km is the average depth (below sea level) of the Moho, ρ_0 is the upper crust-water density contrast (1700 kg/m^3), and $\Delta\rho$ is the density contrast at the Moho (250 kg/m^3). By defining ρ_0 and $\Delta\rho$ in this way we are simulating a layered density structure with a moderate crustal density comprising the topography (2700 kg/m^3 [*Gladczenko et al.*, 1997]), a high-density crust comprising the Moho topography (3050 kg/m^3 [*Gladczenko et al.*, 1997] for mantle density of 3300 kg/m^3), and a flat interface separating the two layers. Moho topography is proportional to $H(k)$ by the ratio $\rho_0/\Delta\rho$ and a flexural term $1/\xi = [1 + Dk^4/\Delta\rho g]^{-1}$, where g is the acceleration of gravity. Flexural rigidity D depends on Young's modulus, $E = 8 \times 10^{10}$ N/m^2, Poisson's ratio, $\nu = 0.25$, and effective elastic plate thickness T_e according to $D = ET_e^3/12(1-\nu^2)$. When D is nonzero, the term $1/\xi$ reduces Moho topography and $B(k)$ relative to the case of Airy isostasy ($T_e = D = 0.0$ and $1/\xi = 1.0$). The physical meaning for the reduction of $B(k)$ is that loading on top of an elastic plate with finite strength causes a smaller (though broader) downward deflection of the Moho than in the case of Airy isostasy in which the elastic plate has zero strength.

Observed Bouguer and free-air gravity profiles are compared with theoretical profiles of Airy isostasy and surface loading with $T_e = 10$ km in Figure 1. Over the Eastern Salient, both of the theoretical Bouguer profiles underpredict the amplitude of the observed anomaly (Figure 1a). Even the Airy isostasy profile under-predicts the variation in Bouguer anomaly by ~30 mGal, or ~20% of the observed anomaly. The above misfit is also evident in comparisons of free-air gravity profiles (Figure 1a). Over the High Plateau the longest-wavelength variation in Bouguer gravity is explained equally well by both models (Figure 1b); that is, $T_e = 10$ km is too weak to reduce the downwarping of the Moho at such a broad wavelength (equation (2)). This finding is consistent with results of *Gladczenko et al.* [1997] and *Sandwell and Renkin* [1988], which indicate that the large-scale topography is compensated by Airy isostasy. Differences between observed and predicted anomalies, however, become apparent near the eastern margin of the plateau (along-track distance of 500-1000 km) where intermediate-wavelength (λ ~ 250-500 km) variations become important. Here the observed anomaly shows a variation ~20-30 mGal greater than the two predicted profiles. This discrepancy is ~15% of the total variation in the Bouguer anomaly and is comparable to the total variation in the free-air gravity (Figure 1b).

The above intermediate-wavelength misfits are robust findings as we found by testing a range of model parameters. Over a range of upper crustal densities of ρ_t = 2600-2900 kg/m^3 (i.e., ρ_0 = 1600-1900 kg/m^3) and lower crustal densities of ρ_b = 2600-3100 kg/m^3 (i.e., $\Delta\rho$ = 200-700 kg/m^3 for a mantle density of 3300 kg/m^3), we were able to reduce but not eliminate the misfits. For example, our best fit model for the Eastern Salient has $\rho_t = \rho_b$ = 2600 kg/m^3. This model predicts a negative Bouguer anomaly with a maximum amplitude greater than that in Figure 1 but still ~20 mGal less than that observed. The amplitude of the Bouguer low is increased in this model because the low crustal density assumed minimizes the predicted crustal thickness (<20 km) and thus the average depth of the compensating mass, z_c ~15 km (see equation (2)). This result implies that any distribution of crustal thickness or density, if in local isostatic equilibrium, would have to occur at an average depth <15 km in order to explain the high-amplitude Bouguer anomaly over the Eastern Salient. This depth is significantly less than that of our preferred model (z_c = 21.7 km) which has a crustal thickness of 30-35 km and densities ρ_t = 2700 kg/m^3 and ρ_b = 3050 kg/m^3 most consistent with values constrained from independent seismic refraction and gravity studies [*Gladczenko et al.*, 1997]. In fact, preliminary results of the seismic refraction experiment of KH98-1 indicate igneous crust as thick as 40 km on the High Plateau [*Araki et al.*, 1998]. Gravity models of a 40-km-thick crust yield even greater misfits than those shown in Figure 1. Thus surface loading models with crustal thicknesses and densities most consistent with available seismic data are unable to explain the intermediate-wavelength gravity anomalies.

We also performed a series of calculations to quantify the effects of sediment thickness variations on the above misfits. Single-channel seismic data taken during the KH98-1 cruise show sediment thickness variations as large as 1 km. Calculations that took into account this sediment thickness variations, however, showed little change in misfits between predicted and observed gravity anomalies at intermediate wavelengths and greater. The sediments are likely to affect misfits only at short wavelengths. We thus conclude that over length scales of 250-500 km, observed Bouguer anomalies of OJP are too high in amplitude be explained by models of only surface loading.

3. Observed Admittance and Coherence

To better determine the wavelength dependence of the gravity anomalies, we analyze subregions of the bathymetry (Plate 1a) and Bouguer anomaly (Plate 2a) maps in the spectral domain. Here we rely on the satellite-derived gravity because it provides uniform coverage over the region and provides the best constraints on long- and intermediate-wavelength anomalies. The reliability of the satellite gravity data is confirmed by comparisons with our ship track free-air data; along line 1, the rms difference between satellite and ship data is 4.64 mGal, and over line 2, the rms difference is 4.47 mGal. To exclude the Solomon islands and regions of OJP most affected by the Solomon trench, we do our analysis on two rectangular subregions, which are outlined in Plates 1 and 2. The sizes and orientations of these subregions were chosen to maximize the areas covered over the Eastern Salient and High Plateau, as well as maximizing symmetry when mirroring bathymetry and Bouguer maps to minimize edge effects in Fourier spectrums. The Fourier spectrums of the subregions were analyzed in two forms: (1) admittance, which is the ratio of Bouguer gravity and topography spectrums; and (2) coherence, which quantifies the correlation between Bouguer gravity and topography spectrums.

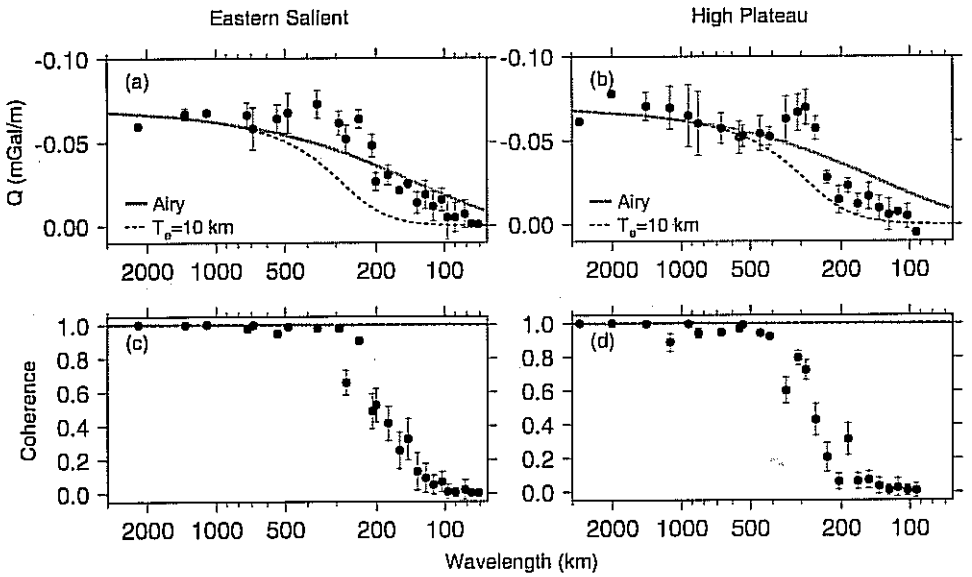

Figure 2. Observed admittance (equation (3), dots) for (a) the Eastern Salient and (b) the High Plateau. The wavelength of each point is the central wavelength within each wave number bin and error bars indicate standard deviations. Also shown are theoretical profiles (equation (2)) assuming Airy isostasy (gray) and surface loading of an elastic plate of thickness, T_e = 10 km (dashed). Coherence between Bouguer gravity and bathymetry maps (equation (4)) for (c) Eastern Salient and (d) High Plateau. The theoretical profiles for Airy isostasy (T_e = 0 km) and T_e = 10 km predict a coherence of 1.0 at all wavelengths.

The two quantities provide independent methods by which to assess the relative importance of surface versus subsurface loads, as well as the effective elastic plate thickness associated with each load type.

Admittance can be estimated from observed Bouguer gravity and bathymetry maps by [*Banks et al.*, 1977; *Lewis and Dorman*, 1970; *McKenzie and Bowin*, 1976; *McNutt and Parker*, 1978]

$$\hat{Q}(k) = \frac{\langle B\,H^* \rangle}{\langle H\,H^* \rangle}, \tag{3}$$

where B and H are the amplitude spectra of the Bouguer and topography subregions, respectively. The asterisks denote complex conjugates and the angle brackets indicate averages over a small range of 2-D wave numbers. Admittance can be thought of as a measure of the ratio of Moho-to-surface topography at a given wavelength.

Coherence is the square of the correlation coefficient between Bouguer gravity and bathymetry in each wave number bin [*Banks et al.*, 1977; *Louden and Forsyth*, 1982; *McKenzie and Bowin*, 1976]:

$$\gamma(k)^2 = \frac{\langle B\,H^* \rangle \langle B\,H^* \rangle}{\langle B\,B^* \rangle \langle H\,H^* \rangle}. \tag{4}$$

To first order, coherence quantifies the statistical relationship between Moho and surface topography. In the case of Airy isostasy as well as surface loading of an elastic plate, each wavelength of surface topography causes an undulation in Moho topography and the resulting coherence is predicted to be unity.

Figures 2a and 2b compare observed (equation (3)) and predicted (equation (2)) admittance functions over the range of wavelengths considered in each of the two study areas. At the greatest wavelengths (>700 km) the models are indistinguishable and both predict admittance values of ~-0.06 to -0.07 mGal/m as consistent with the observed values. This result is the same as that obtained from the analysis of the long-wavelength Bouguer anomaly profile over the High Plateau. At intermediate wavelengths (250-500 km) the admittance functions become greater in magnitude than predicted by Airy isostasy and peak in amplitude at λ ~ 250-350 km. These features are another indication of the intermediate-wavelength misfits between the shipboard and predicted gravity profiles. Finally, for λ <~200 km, absolute values of the observed admittance become less than the Airy curve and eventually taper to zero. A decrease in admittance at intermediate and short wavelengths is predicted by surface loading of an elastic plate (equation (2)); however, the example shown for T_e = 10 km predicts a more rapid decrease than observed.

Figures 2c and 2d show observed coherence functions for the Eastern Salient and High Plateau, respectively. At the greatest wavelengths, coherence is very high and near 1.0, which is again consistent with local isostatic compensation. At intermediate wavelengths, however, the coherence drops to near zero over a relatively narrow range of wavelengths. Over the Eastern Salient the decrease in coherence occurs over λ = 150-350 km, values slightly less than λ = 200-450 km, over which coherence of the High Plateau decreases. This decrease in coherence cannot be explained by models of Airy isostasy or surface loading on an elastic plate of a single elastic plate thickness. A more complex loading history is required.

4. Models of Surface and Subsurface Loading

A successful model for the compensation mechanism and thus loading history of the Ontong Java Plateau must explain two characteristics of the Bouguer gravity and bathymetry spectrums for λ ~ 250-500 km: (1) admittance values (and Bouguer

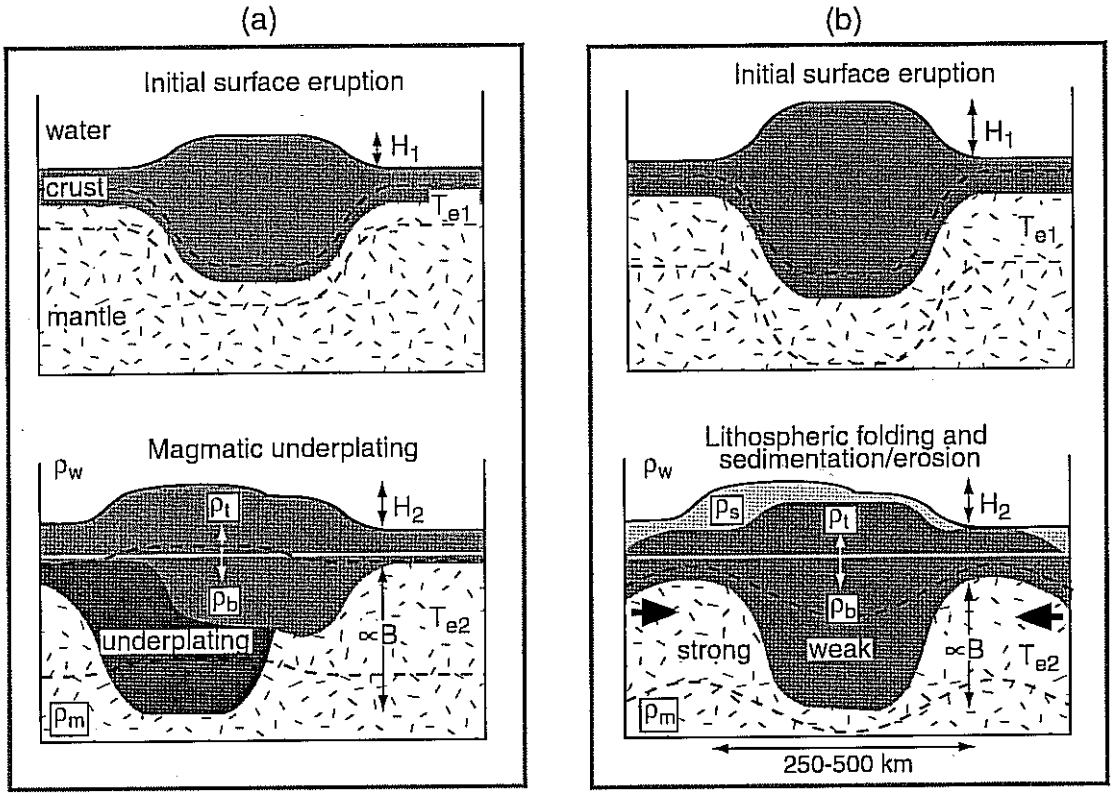

Figure 3. Cartoons showing two possible loading histories for Ontong Java Plateau. The density structure assumed in models have a layer of water, $\rho_w = 1000$ kg/m^3; a layer of upper crust $\rho_t = 2700$ kg/m^3 (edifice material above white line); and layer of lower crust $\rho_b = 3050$ kg/m^3 (crust below white line); and mantle $\rho_m = 3300$ kg/m^3. (a) Late stage underplating model: (top) Volcanic crust emplaced during the first eruptive phase (gray) loads the surface of a thin elastic plate ($T_{e1} = 4$-6 km) represented schematically by dashed curves. (bottom) At a later time, magmatic intrusions (dark shading) push upward on and deform a thick plate (dashed curves, $T_{e2} = \sim 30$ km). Bouguer gravity (B) is proportional to Moho topography. (b) Lithospheric folding model: (top) All of the volcanic crust is emplaced on an elastic plate of moderate thickness ($T_{e1} = 15$ km). (bottom) Tectonic compression (bold arrows) causes the lithosphere to fold as shown schematically by dashed curves. Downward bending occurs where topography is high because the strong mantle lithosphere is already bowed down by the weight of the relatively weak lower crust. Sedimentation and/or eroded material (light shading, with sediment-water density contrast $\rho_s = 700$ kg/m^3) is uncorrelated with the igneous crust.

anomalies) are greater in magnitude than predicted by Airy isostasy and (2) coherence drops from 1.0 to 0.0. Here we examine two alternative models, both of which involve a multiple loading history with surface and subsurface loads.

4.1. Late Stage Magmatic Underplating

The first model involves an initial phase of volcanism which loads the surface of a young and thin elastic lithosphere (Figure 3a). This stage is followed by a second phase of volcanism in the form of intrusions that underplate the original crust and thus load an older and thicker elastic plate from below. The underplated crust is less dense than the surrounding mantle and therefore pushes upward on the lithosphere; however, an increase in topography is inhibited by the thick elastic plate. The resulting structure yields a greater Bouguer anomaly than predicted by Airy isostasy. Furthermore, if underplating is uncorrelated with the crust emplaced during the first magmatic phase, then coherence between Bouguer gravity and topography would be low for wavelengths shorter than the characteristic flexural wavelength of the lithosphere during underplating.

Calculation of admittance and coherence functions for this model is identical to previous treatments of a load on the top of an elastic plate combined with a buoyant load from below [e.g., *Forsyth*, 1985]. For a given wave number, the topography $H(k)$ is the result of combined contributions from the initial surface loaded magmas, $H_1(k)$, and the topography resulting from underplating, $H_2(k)$; $H(k) = H_1(k) + H_2(k)$. The admittance function $Q_1(k)$ for the surface load is given by equation (2), in which the filter $1/\xi$ is a function of the elastic plate thickness during surface loading, T_{e1}. The admittance function for the subsurface load is [*Forsyth*, 1985; *McNutt*, 1983]

$$Q_2(k) = -2\pi G\rho_0 \exp(-kz_c)\phi, \qquad (5)$$

where the function $\phi = [1 + Dk^4/\rho_0 g]$ depends on the elastic plate thickness during subsurface loading T_{e2}. In contrast to $1/\xi$, which reduces admittance for top loading, ϕ amplifies admittance, reflecting the fact that a larger subsurface load (i.e., Moho topography) is required to generate a given topography due to the inhibiting effects of the elastic plate. The total Bouguer anomaly is $B = (Q_1H_1 + Q_2H_2)$ and thus the theoretical value for $Q(k)$ from equation (3) is [*Forsyth*, 1985]

$$\hat{Q}(k) = \frac{\langle (Q_1 H_1 + Q_2 H_2)(H_1 + H_2) \rangle}{\langle (H_1 + H_2)(H_1 + H_2) \rangle}$$

$$= \frac{\langle Q_1 H_1^2 + Q_2 H_2^2 \rangle}{\langle H_1^2 + H_2^2 \rangle}. \quad (6)$$

Here we have assumed that surface and subsurface loads are uncorrelated, and thus averaging over phases and wave numbers eliminates the terms involving $H_1 H_2$. If we assume the volume of underplating divided by the volume of surface loaded crust is a fraction f, then $H_2 = f\beta H_1$, where $\beta = (\rho_0/\Delta\rho\xi + 1)/(\phi\rho_0/\Delta\rho + 1)$; and combined with (2) and (5), (6) becomes

$$\hat{Q}(k) = -2\pi G\rho_0 \exp(-kz) \frac{(1/\xi + \varphi f^2\beta^2)}{(1 + f^2\beta^2)}. \quad (7)$$

Note that if only surface loading occurs ($f = 0$), (7) reduces to equation (2); but if f is nonzero, then $Q(k)$ can be larger than predicted by Airy isostasy depending on the values of ξ, ϕ, and $f\beta$.

Similarly, the theoretical coherence after (4) is [*Forsyth*, 1985]

$$\gamma(k)^2 = \frac{\langle Q_1 H_1^2 + Q_2 H_2^2 \rangle^2}{\langle Q_1^2 H_1^2 + Q_2^2 H_2^2 \rangle \langle H_1^2 + H_2^2 \rangle}, \quad (8)$$

again assuming incoherent subsurface and surface loading. Combining (2), (5) and the relation $H_2 = f\beta H_1$,

$$\gamma(k)^2 = \frac{(1/\xi + \varphi f^2\beta^2)^2}{(1/\xi^2 + \varphi f^2\beta^2)(1 + f^2\beta^2)}. \quad (9)$$

If only surface loading occurs ($f = 0$), coherence will be 1.0; but if subsurface loading is important then coherence will decrease to zero at wavelengths controlled by the elastic thickness during underplating, T_{e2}.

Figures 4a and 4b compare observed admittance functions with predictions of (7) for different values of T_{e1}, T_{e2}, and f. Over the Eastern Salient the maximum amplitude of the intermediate-wavelength admittance is best explained by a volume of underplating 1-2 times (i.e., $f = 1$-2) that of the surface load (Figure 4a). The wavelength of the peak admittance is sensitive to elastic plate thickness at the time of underplating (T_{e2}) and is well explained by a relatively thick plate of $T_{e2} = 30$ km. In contrast, the decrease in admittance at short wavelengths is sensitive to the elastic plate thickness during surface loading (T_{e1}). Only a thin plate ($T_{e1} = 4$ km) is required. Theoretical curves with similar parameters match the admittance functions of the High Plateau. The only difference is the more rapid decrease in admittance at short wavelengths, suggesting that surface loading occurred on a slightly thicker elastic plate of $T_{e1} = 6$ km (Figure 4b).

Comparison of observed coherence functions with predictions of (9) also suggests substantial subsurface loading of OJP beneath a thick elastic plate. Over the Eastern Salient the decrease in coherence at $\lambda = 150$-350 km is well explained by theoretical profiles of $T_{e2} = 20$-30 km and $T_{e1} = 4$ km for $f = 2$. Over the High Plateau the drop in coherence occurs at $\lambda = 200$-450 km, suggesting slightly higher average plate thicknesses ($T_{e2} = 30$ and $T_{e1} = 6$ km) with the same fraction $f = 2$. Lower values of f predict higher coherence at short wavelengths and begin to misfit the observations. Thus both the admittance and coherence data can be explained by models in which OJP is compensated by a combination of surface loading on a thin elastic plate and subsurface loading, in the form of a buoyant load, beneath a thick elastic plate.

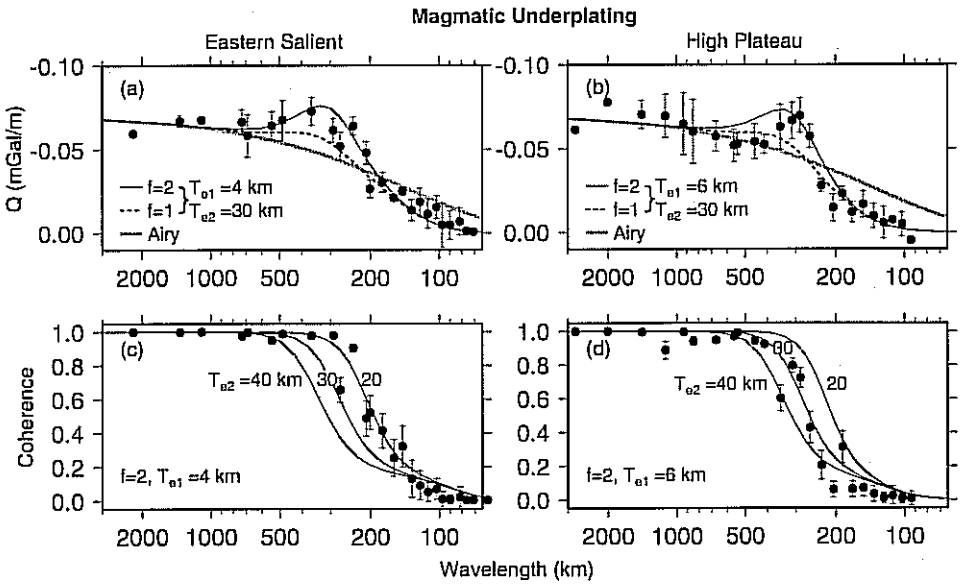

Figure 4. Observed admittance (dots) and predictions for (a) the Eastern Salient and (b) the High Plateau. Gray curve is the Airy isostasy model for reference. Solid curve (equation (7)) assumes that the subsurface load is twice the volume of the surface load ($f = 2$), and dashed curve assumes $f = 1$. Subsurface loading occurs on an elastic plate of thickness $T_{e2} = 30$ km. Elastic plate thickness during the surface load is $T_{e1} = 4$ km in Figure 4a and $T_{e1} = 6$ km in Figure 4b. Observed coherence (dots) and predictions for (c) Eastern Salient and (d) High Plateau. Theoretical curves (equation (9)) assume $f = 2$, for $T_{e2} = 20$, 30, and 40 km as labeled. $T_{e1} = 4$ km in figure 4c and $T_{e1} = 6$ km in Figure 4d.

4.2. Recent Lithospheric Folding

The second model that we consider involves an initial surface loading in which all of OJP's volcanic crust was emplaced upon an elastic lithosphere of moderate strength (Figure 3b). This volcanic loading is then followed by a subsurface load in the form of lithospheric folding. Such folding could be the result of tectonic compression associated with the collision of OJP and the Solomon trench [*Kroenke*, 1972, 1996; *Petterson et al.*, 1997]. Folding could explain the high admittance values if folding occurred at intermediate wavelengths and was correlated with the initial volcanic topography such that downward folding coincided with preexisting topographic highs and upward folding occurred at topographic lows. Correlated folding alone, however, would predict high coherence at all wavelengths. To explain the low coherence, this model therefore requires an additional load, uncorrelated with the volcanic structure. Such a load could be sedimentation and erosion.

We model the effects of correlated folding and uncorrelated sedimentation/erosion as follows. At a given wave number k the topography of the volcanic crust underneath the sediments is $H_v(k)$. This quantity is the sum of the original topography that formed when OJP first erupted, $H_1(k)$, and the topography due to lithospheric folding. Assuming the amplitude of folding is a fraction $F(k)$ of $H_1(k)$, then

$$H_v(k) = H_1(k)[1\text{-}F(k)]. \tag{10}$$

Here $F(k)$ is assumed to be a Gaussian function, $F(k) = F_0\exp[-(k - k_0)^2/\sigma^2]$, with parameters set arbitrarily such that the Gaussian is centered on a wavelength $\lambda_0 = 280$ km ($k_0 = 2\pi/\lambda_0$) and has a width controlled by $\sigma = 0.1068$ km^{-1}. $F(k)$ is subtracted in (10), indicating folding reduces the original topography. The predicted free-air anomaly due to the volcanic crust is therefore

$$Faa_1(k) = 2\pi G\left[\exp(-kz_t)\rho_0\left(1 - F(k)\right)\right.$$
$$\left. - \exp(-kz_c)\left(\rho_0/\xi_1 + \Delta\rho F(k)\right)\right]H_1(k) \tag{11}$$

where z_t is the average depth of $H_v(k)$, and $1/\xi_1$ is the filter due to plate flexure, which depends on the elastic plate during initial volcanic loading, T_{e1}. The first term is the contribution of volcanic topography and the second term is the contribution from the Moho, noting that folding adds a small amount to Moho topography.

Sedimentation and erosion contribute additional topography $H_2(k)$ and the free-air gravity signal:

$$Faa_2(k) = 2\pi G\left[\exp(-kz_t)\rho_s - \left\{\exp(-kz_t)(\rho_0 - \rho_s)\right.\right.$$
$$\left.\left. + \exp(-kz_c)\Delta\rho\right\}\frac{\rho_s}{\Delta\rho_s}\frac{1}{\xi_2}\right]H_2(k), \tag{12}$$

where ρ_s is the sediment-water density contrast (700 kg/m^3) and $\Delta\rho_s$ is the sediment-mantle density contrast (1600 kg/m^3). Sedimentation/erosion is loading the surface of an effective elastic plate of thickness T_{e2}, which determines the filter $1/\xi_2$. The first exponential term is the contribution from the sediment-water interface, the second exponential term is the signal from the sediment-crust interface, and the last term is the contribution from Moho topography. The total free-air anomaly is the sum of (11) and (12). The predicted Bouguer anomaly, as we have calculated from the data, removes the effects of the total topography assuming a density of ρ_0,

$$B(k) = [Faa_1(k) + Faa_2(k)]$$
$$- 2\pi G\exp(-kz_t)\rho_0[(1 - F(k))H_1(k) + H_2(k)]. \tag{13}$$

With (11) and (12), (13) becomes $B = (Q_1H_1 + Q_2H_2)$, where

$$Q_1(k) = -2\pi G\exp(-kz_c)\left[\rho_0/\xi_1 + \Delta\rho F(k)\right], \tag{14}$$

and

$$Q_2(k) = -2\pi G\left[\exp(-kz_t)(\rho_0 - \rho_s)\right.$$
$$\left. + \left\{\exp(-kz_t)(\rho_0 - \rho_s) + \exp(-kz_c)\Delta\rho\right\}\frac{\rho_s}{\Delta\rho_s}\frac{1}{\xi_2}\right]. \tag{15}$$

Thus the theoretical function $Q(k)$ takes on a form similar to (6):

$$\hat{Q}(k) = \frac{\left\langle (Q_1H_1 + Q_2H_2)(H_1(1 - F(k)) + H_2)\right\rangle}{\left\langle (H_1(1 - F(k)) + H_2)(H_1(1 - F(k)) + H_2)\right\rangle}. \tag{16}$$

Parameterizing sedimentation/erosional topography as a fraction f_s of the original volcanic topography $H_2(k) = f_sH_1(k)$ and assuming no correlation between sedimentation/erosion and volcanic topography, the final equation is

$$\hat{Q}(k) = \frac{\left\langle (Q_1(1 - F(k)) + Q_2f_s^2\right\rangle}{\left\langle (1 - F(k))^2 + f_s^2\right\rangle}. \tag{17}$$

Here we assume $f_s = 0.1$. Following the same reasoning, the theoretical coherence function is similar to (8), and its final form is

$$\gamma(k)^2 = \frac{\left\langle (Q_1(1 - F(k)) + Q_2f_s^2\right\rangle^2}{\left\langle (1 - F(k))^2 + f_s^2\right\rangle\left\langle Q_1^2 + Q_2^2f_s^2\right\rangle}. \tag{18}$$

Figure 5 compares observed admittance and coherence functions with predictions of (17) and (18) using a set of reference parameters. The amplitude of admittance at intermediate and short wavelengths is predicted to be most sensitive to the folding amplitude F_0 and elastic plate thickness during initial volcanism T_{e1}. Admittance is predicted to increase with F_0 because larger folding reduces intermediate-wavelength topography to a greater degree; admittance is predicted to decrease with increasing T_{e1} because a stronger plate allows less Moho topography for a given surface load. The observed admittance data for the Eastern Salient and High Plateau can be explained by predictions for $F_0 = 0.65$-0.75 and $T_{e1} = 15$ km (Figure 5a and 5b). The admittance data could also be explained by lower values of $F_0 = 0.3$-0.4 and $T_{e1} = 5$ km.

Coherence, however, provides additional constraints (Figure 5c and 5c). The wavelengths at which coherence is predicted to drop is sensitive T_{e1} and insensitive to T_{e2} because the term involving T_{e2} in (15) is small, and thus Q_2 is dominated by the first exponential term. The observed drop in coherence over $\lambda \sim$ 150-350 km for the Eastern Salient suggests a moderate plate thickness, more consistent with $T_{e1} = 15$ km. Smaller values of T_{e1} would predict the drop in coherence to occur at shorter wavelengths and therefore would fail to explain the observed coherence. The drop in coherence for the High Plateau begins at wavelengths slightly greater than predicted by our models, a detail not well explained by the range of parameters tested. Nonetheless, this model of lithospheric folding provides a

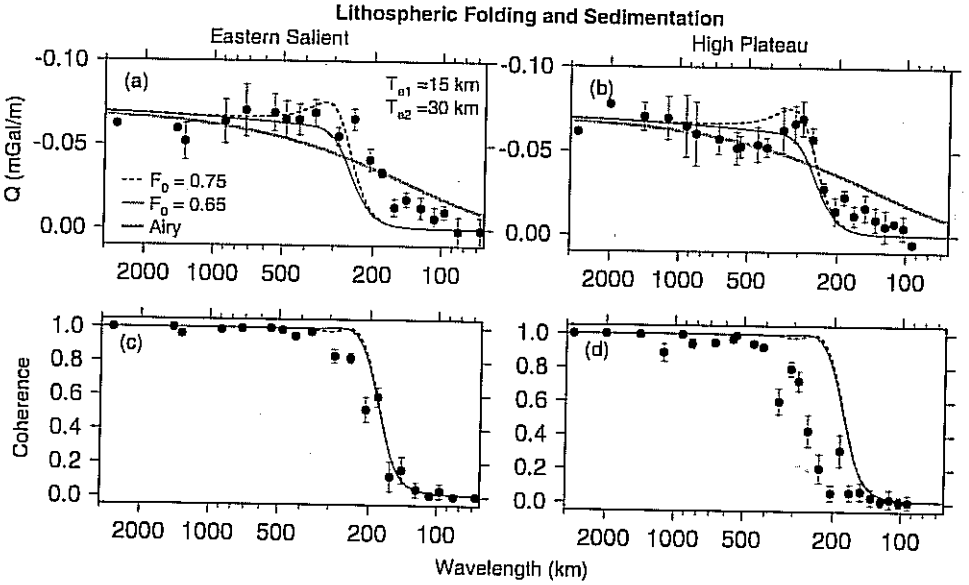

Figure 5. Same as Figure 4 but with predictions of lithospheric folding model. Admittance curves are from equation (17); coherence curves are from equation (18). All predictions are derived by assuming that the surface eruption loads an elastic plate of thickness T_{e1} = 15 km, sedimentation/erosion loads a plate of average thickness T_{e2} = 30 km, and maximum folding occurs at a wavelength of 280 km with amplitude, F_0 = 0.65-0.75.

reasonable explanation for the prominent features of the admittance and coherence observations.

5. Discussion

The observed admittance and coherence functions indicate that the major constructs of OJP experienced a phase of large-scale deformation after the initial phase of volcanism. On the basis of the admittance and coherence data alone, both the magmatic underplating and lithospheric folding models are possible. Here we discuss the potential causes and implications of each model as well as additional constraints.

5.1. Lithospheric Folding

Models of lithospheric folding have been proposed for a number of continental settings in tectonic compression based on similar analyses of admittance and coherence [e.g., *Jin et al.*, 1994; *Stephenson and Lambeck*, 1985; *Zuber et al.*, 1989]. Evidence for folding of oceanic lithosphere has also been documented in the northeast Indian ocean [*Geller et al.*, 1983; *McAdoo and Sandwell*, 1985]. Indeed, OJP is now in a compressional tectonic setting due to its collision with the Solomon arc [*Petterson et al.*, 1997]. The folding model for OJP has two primary requirements: (1) lithospheric folding occurred over a limited range of intermediate wavelengths (~250-500 km) and (2) lithosphere folding is highly correlated with preexisting volcanic structure.

The first requirement can be explained in the context of models of a folding plastic layer [e.g., *Martinod and Davy*, 1992; *McAdoo and Sandwell*, 1985; *Zuber*, 1987]. *McAdoo and Sandwell* [1985] demonstrated that a thin elasto-plastic layer under lateral compression will fold at a characteristic wavelength, controlled by its thickness. Folding wavelengths of 250-500 km suggest a very thick and thus old lithospheric plate during folding of OJP. This requirement is consistent with the fact that the seafloor near OJP is old (130-160 m.y. [*Nakanishi et al.*, 1989]), the collision with the Solomon trench was relatively recent (~20-25 Ma [*Petterson et al.*, 1997]), and the most intense compression is even more recent (2-4 Ma [*Petterson et al.*, 1997]).

The second requirement that folding occurred in phase with preexisting volcanic structure could be the consequence of a layered rheological structure of the lithosphere. OJP's thick crust may result in a lower basaltic layer that is weak compared to a strong, rigid layer of the surrounding peridotite [e.g., *Burov and Diament*, 1995]. Before folding, the strong mantle layer would have already been bowed downward beneath areas of local crustal thickness maxima (Figure 3b) such as the Eastern Salient. Consequently, when tectonic compression began, these preexisting folds grew. In this way, initial crustal structure and folding might be strongly coupled but still subject to the characteristic folding wavelength of a rheologically layered lithosphere [*Martinod and Davy*, 1992].

A simple folding model would predict linear gravity highs and lows such as observed in the Indian Ocean [*McAdoo and Sandwell*, 1985]. To examine this possibility, we generate a residual Bouguer gravity anomaly by subtracting from the observed Bouguer gravity map, the Bouguer anomaly that is predicted by assuming Airy isostasy. Variations in this residual anomaly (Plate 2b) reveal the spatial pattern of deviations from the Airy isostasy model (we reemphasize that only the bathymetry and Bouguer anomalies within the outlined subregions were used in our admittance and coherence analysis). A high-amplitude residual gravity high is evident just north of and parallel to the Solomon trench. At least part of this high could be the flexural bulge remaining from when the Pacific plate was subducting at the Solomon trench (now the Australian plate is subducting [*Petterson et al.*, 1997]). Just NE of this high is a gravity low that is most linear over the Eastern Salient. Over the High Plateau and on to the Nauru Basin, there is a pattern of undulations that appear elongate in the NW-SE direction. Similar undulations are also evident in the free-air gravity

anomaly (Plate 1b). We also note that many of the elongate features are broken by variations along them which, if caused by folding, would suggesting a component of compression parallel to the elongations. Nonetheless, the prominent fabric is parallel to the Solomon trench/arc system. This pattern is consistent with a folding model with compression perpendicular to the Solomon trench.

The importance of this folding model is that it suggests that OJP and the underlying lithosphere are still supporting substantial compressive stress. This possibility has ramifications on the form of subduction at the Solomon arc as well as the ability of large oceanic plateaus like OJP to subduct [*Kroenke*, 1972; *Petterson et al.*, 1997]. Such large compressive stresses may also have a role in a recent change in direction and rate of Pacific plate motion [*Wessel and Kroenke*, 1997].

5.2. Magmatic Underplating

Magmatic underplating has been proposed by previous workers to explain the high seismic velocities throughout thick sections of the lower crust at OJP [*Coffin and Eldholm*, 1993; *Hussong et al.*, 1979; *Neal et al.*, 1997]. Similar observations at other flood basalt provinces [*Coffin and Eldholm*, 1993] as well as oceanic hotspots [*Caress et al.*, 1995; *ten Brink and Brocher*, 1987] suggest that magmatic underplating may be fundamental to the accretion process of many large igneous provinces. A new aspect of our model is that it requires underplating to have occurred beneath a much thicker elastic plate (T_{e2} = 20-30 km) than during surface loading (T_{e1} = 4-6 km). A second new result is that our model suggests the volume fraction (f = 1-2) of the subsurface load could have been as large or larger than the initial surface eruption.

These two new constraints suggest that Ontong Java formed by two or more major magmatic events. The first event was most likely the eruption of the 122 Ma magmas [*Mahoney et al.*, 1993; *Tejada et al.*, 1996]. The thin elastic plate during initial loading (T_{e1} = 4-6 km) as required by our models is consistent with this initial eruption occurring on young seafloor, near a ridge axis [*Mahoney and Spencer*, 1991; *Winterer and Nakanishi*, 1995]. The high values of T_{e2} required for the subsurface load suggest that the subsequent subsurface loading event(s) occurred beneath a much older lithosphere. Thus underplating may have occurred significantly later than the initial surface load. The widespread magmatism dated at 90 Ma is a strong candidate for this event [*Mahoney et al.*, 1993; *Tejada et al.*, 1996], although another magmatic event on the OJP island of Malaita is documented at ~44 Ma [*Tejada et al.*, 1996]. In a strict sense, this late stage subsurface load could be any source of buoyancy that generates permanent uplift of the preerupted crust. This could be magmatic underplating, as we have discussed, but could also be low-density mantle residuum of partial melting [e.g., *Phipps Morgan et al.*, 1995; *Saltzer and Humphreys*, 1997]. Both of the above sources imply a large melting event well after the initial eruption of OJP. We also note that it is not possible to distinguish between a single late stage event or several late stage events, nor can we constrain the duration of this later event(s).

With regard to this model the residual gravity anomalies in Plate 2b over the Eastern Salient and High Plateau would indicate the pattern of underplated material not locally compensated. The prominent residual gravity low over the Eastern Salient would suggest that underplating was substantial beneath the whole edifice. The intermediate-wavelength features over the High Plateau suggest a pattern of underplating that is strong at intermediate wavelengths. At this point, we are unable to assess the importance of underplating at longer wavelengths because T_{e2} only affects intermediate wavelengths and shorter. This is important to note because in our above models we assume that underplating is equally voluminous at all wavelengths and thus we require a substantial underplating volume (f = 1-2) to explain the admittance and coherence data. Because of this assumption the volumes predicted by our models could be upper bounds.

Independent evidence from plateau subsidence, however, suggests that underplating at long wavelengths may, in fact, be substantial. *Ito and Clift* [1998] used Ocean Drilling Program/Deep Sea Drilling Project (ODP/DSDP) drill core records to estimate the tectonic subsidence of OJP and found that the total subsidence since eruption was 1-2 km less than predicted by thermal models of hotspot-influenced lithosphere. This could be explained by a scenario in which the net subsidence was a superposition of thermal contraction of the lithosphere as well as uplift due to late stage underplating. The broad spatial distribution of the drill sites (Plates 1 and 2) suggests that this uplift occurred over the whole plateau and was not confined to just intermediate wavelengths. Indeed, our models predict underplating to contribute 0.6-1.7 km of additional topography at the drill sites studied (sites 288, 289, 807, Plate 1), a range consistent with the 1-2 km suggested by *Ito and Clift* [1998]. Thus, if all of the subsurface loaded material is underplated magmas that occurred at all wavelengths, then our model implies that 50-66% (f = 1-2 times the surface load) of the present-day crustal volume is underplated material. This estimate is similar to *Ito and Clift* 's [1998] estimate of 50%. Additionally, if only a fraction of the crust was emplaced during the initial magmatic phase, then this would explain why most of OJP remained below sea level [*Kroenke et al.*, 1991] unlike most hotspot volcanoes. Finally, the uplift associated with underplating may have caused many of the large-scale normal faults documented along the margins of OJP [*Kroenke*, 1972].

In light of the subsidence constraints, the lithospheric folding model would also predict anomalously low subsidence at sites 288 and 807, which are located on residual gravity highs (Plate 2b), areas that presumably have been uplifted by folding. Because site 288 is located on the most positive residual gravity anomaly, folding would predict this site to have experienced the least subsidence; this site, however, shows the most subsidence [*Ito and Clift*, 1998]. Moreover, folding would predict anomalously high subsidence at site 289, but this site appears to have subsided the least of the three drill sites. The folding model, which predicts late stage deformation only at intermediate wavelengths, is therefore inconsistent with the sediment data. For this reason we favor the underplating model.

5.3. Implications

A popular hypothesis for the origin of this and other large igneous provinces is that they formed by the rapid ascent and melting of the leading head of a new mantle plume [*Campbell and Griffiths*, 1990; *Richards et al.*, 1989]. The voluminous late stage magmatic event or events proposed by our underplating model adds complexity to this simple model. In fact, multiple-stage accretion is common among many igneous provinces such as the Kerguelen Plateau [*Weis and Frey*, 1996], the Crozet Bank [*Goslin and Diament*, 1987], the Austral-Cook volcano chain [*Diament and Baudry*, 1987; *McNutt et al.*, 1997], and the North Atlantic igneous province [*Saunders et al.*, 1997]. A simple explanation for a two-stage accretion is the surfacing of two plume heads as proposed by *Bercovici and Mahoney* [1994]. A subtle weakness of this scenario, however, is that *Bercovici and*

Mahoney [1994] predict the second plume head to be the smaller of the two, whereas our model suggests that the second plume head may have been as, or even more voluminous as the first.

The possibility of more than two eruptive phases or a prolonged second eruptive phase could be explained by the melting of a plume head (or heads) followed by a long-lived mantle plume such as those associated with the Ninetyeast Ridge-Kerguelen Plateau [*Frey and Weis*, 1995; *Weis and Frey*, 1996], the North Atlantic province-Iceland [*Saunders et al.*, 1997], and the Rio Grande Rise-Walvis Ridge-Tristan [*O'Connor and Duncan*, 1990] volcanic systems. For such a long-lived source to erupt on OJP, very little plate motion relative to the source is required. Indeed, the Pacific plate is predicted to have been nearly stationary with respect to the hotspot reference frame during the period 120-90 Ma [*Neal et al.*, 1997]. This would allow for numerous stages of volcanism at OJP over a 30 m.y. period; however, rapid motion of the plate since 90 Ma would not allow for more recent events from a single mantle plume, fixed in the hotspot reference frame. Another possibility for multiple magmatic episodes is the passage of OJP over another hotspot such as Samoa [*Tejada et al.*, 1996]. Alternative scenarios to a hotspot origin of late stage, intraplate magmatism include eruptions controlled by lithospheric stresses [*Hieronymus and Bercovici*, 1999; *McNutt et al.*, 1997; *Sandwell et al.*, 1995] or induced by shallow, small-scale convection [*Buck and Parmentier*, 1986; *Haxby and Weissel*, 1986; *Tackley and Stevenson*, 1993]. These mechanisms, however, may be a less likely source of the late stage magmatism at OJP given the large volume of magma that our models appear to require. Regardless of the mechanism, the high volume of late-stage underplating that the bathymetry, gravity, and subsidence data appear to require casts serious doubt on scenarios involving only one major magmatic event. This conclusion implies that eruption rates may have been appreciably less than previously proposed [*Tarduno et al.*, 1991].

6. Conclusions

Analysis of bathymetry data together with satellite-derived and shipboard gravity of Ontong Java Plateau shows that at long wavelengths, topography is fully compensated. At intermediate wavelengths, however, the Bouguer anomalies are higher in amplitude than predicted by models of Airy isostasy or a single surface loading event. This result is also evident in high-amplitude admittance values at intermediate wavelengths. In addition, coherence between Bouguer gravity and bathymetry spectrums drops to zero at intermediate wavelengths. One explanation for the admittance and coherence data is that the plateau deformed by lithospheric folding, possibly associated with the recent collision of OJP with the Solomon trench. An alternative possibility is a scenario in which surface loading occurred on thin (T_{e1} = 4-6 km) and young lithosphere, while subsurface loading occurred on thicker (T_{e2} = 20-30 km) and older lithosphere. This second possibility suggests an accretion scenario in which an initial surface eruptive phase (122 Ma) was followed by one (90 Ma) or more later stages of magmatism involving magmatic underplating. This model suggests that surface loading magmas could comprise as little as 33-50% of the total present-day crustal volume with as much as 50-66% composed of late stage underplated material. On the basis of our gravity and bathymetry data alone, both models are possible; however, the underplating model is more consistent with independent constraints on plateau subsidence. The multiple accretion scenario proposed supports a double plume head hypothesis as well as the possibility of other mechanisms of intraplate volcanism on OJP.

Acknowledgments. This study was supported by JOI/USSP, ODP Site Augmentation grant JSC 3-98, the University of Hawaii, SOEST Young Investigator Program, and NSF grant OCE-97-30673. We owe the success of cruise KH98-1 to the crew of the R/V *Hakuho-Maru* and we thank K. Mochizuki for his assistance in acquiring the shipboard data. This paper benefited greatly from discussions with F. Martinez and B. Taylor, comments on a prior version of this manuscript by C. Neal and R. Larson, and conscientious reviews by an anonymous reviewer, M. Diament, and the Associate Editor, K. Louden.

References

Araki, E., K. Mochizuki, K. Suyehiro, A. Taira, S. Yoneshima, M. Shinohara, S. Miura, and R. Hino, Seismic structure of Ontong Java Plateau crust, *Eos Trans. AGU., 79*(45), Fall Meet. Suppl., F869, 1998.

Banks, R. J., R. L. Parker, and S. P. Huestis, Isostatic compensation on a continental scale: Local versus regional mechanisms, *Geophys. J. R. Astron. Soc., 51*, 431-452, 1977.

Bercovici, D., and J. Mahoney, Double flood basalts and plume head separation at the 660-kilometer discontinuity, *Science, 266*, 1367-1369, 1994.

Buck, W. R., and E. M. Parmentier, Convection beneath young oceanic lithosphere: Implications for thermal structure and gravity, *J. Geophys. Res., 91*, 1961-1974, 1986.

Burov, E. B., and M. Diament, The effective elastic thickness (Te) of continental lithosphere: What does it really mean?, *J. Geophys. Res., 100*, 3905-3927, 1995.

Campbell, I. H., and R. W. Griffiths, Implications of mantle plume structure for the evolution of flood basalts, *Earth Planet. Sci. Lett., 99*, 79-93, 1990.

Caress, D., M. K. McNutt, R. S. Detrick, and J. C. Mutter, Seismic imaging of hotspot-related crustal underplating beneath the Marquesas Islands, *Nature, 373*, 600-603, 1995.

Coffin, M. F., and O. Eldholm, Scratching the surface: Estimating dimensions of large igneous provinces, *Geology, 21*, 515-518, 1993.

Diament, M., and N. Baudry, Structural trends in the southern Cook and Austral archipelagoes (south central Pacific) based on an analysis of Seasat data: Geodynamic implications, *Earth Planet. Sci. Lett., 85*, 427-438, 1987.

Dorman, L. M., and B. T. R. Lewis, Experimental isostasy, 1, Theory of the determination of the earth's isostatic response to a concentrated load, *J. Geophys. Res., 75*, 3357-3365, 1970.

Forsyth, D. W., Subsurface loading and estimates of the flexural rigidity of continental lithosphere, *J. Geophys. Res., 90*, 12,623-12,632, 1985.

Frey, F., and D. Weis, Geochemical constraints on the origin and evolution of the Ninetyeast Ridge: A 5000 km hotspot trace in the eastern Indian Ocean, *Contrib. Mineral. Petrol., 121*, 18-28, 1995.

Geller, C. A., J. K. Weissel, and R. N. Anderson, Heat transfer and intraplate deformation in the central Indian Ocean, *J. Geophys. Res., 88*, 1018-1032, 1983.

Gladczenko, T. P., M. F. Coffin, and O. Eldholm, Crustal structure of the Ontong Java Plateau: Modeling of new gravity and existing seismic data, *J. Geophys. Res., 102*, 22,711-22,729, 1997.

Goslin, J., and M. Diament, Mechanical and thermal isostatic response of the Del Cano Rise and Crozet Band (southern Indian Ocean) from altimetry data, *Earth Planet. Sci. Lett., 84*, 285-294, 1987.

Haxby, W. F., and J. K. Weissel, Evidence for small-scale mantel convection from Seasat altimeter data, *J. Geophys. Res., 91*, 3507-3520, 1986.

Hieronymus, C. F., and D. Bercovici, Discrete alternating hotspot islands formed by interaction of magma transport and lithospheric flexure, *Nature, 397*, 604-607, 1999.

Hussong, D. M., L. K. Wipperman, and L. W. Kroenke, The crustal structure of the Ontong Java and Manihiki oceanic plateaus, *J. Geophys. Res., 84*, 6003-6010, 1979.

Ito, G., and P. Clift, Subsidence and growth of Pacific Cretaceous plateaus, *Earth Planet. Sci. Lett., 161*, 85-100, 1998.

Jin, Y., M. K. McNutt, and Y. Zhu, Evidence from gravity and topography data for folding of Tibet, *Nature, 371*, 669-674, 1994.

Kroenke, L. W., Geology of the Ontong Java Plateau, Hawaii Inst. of Geophys. Rep. *72-5*, 119 pp., Honolulu, 1972.

Kroenke, L. W., Plate tectonic development of the western and southwestern Pacific: Mesozoic to present", *The Origin and Evolution of Pacific Island Biotas, New Guinea to Eastern Polynesia: Patterns and Processes*, edited by A. Keast and S. E. Miller, SPB Acad, pp. 19-34, Amsterdam, Netherlands, 1996.

Kroenke, L. W., et al., Proceedings of the Ocean Drilling Program Initial Reports, vol. 130, Ocean Drill Program, College Station, Tex., 1991.

Larson, R. L., Latest pulse of Earth: Evidence for a mid-Cretaceous superplume, *Geology*, *19*, 547-550, 1991.

Lewis, B. T. R., and L. M. Dorman, Experimental isostasy, 2, An isostatic model for the United States derived from gravity and topographic data, *J. Geophys. Res.*, *75*, 3367-3386, 1970.

Louden, K. E., and D. W. Forsyth, Crustal structure and isostatic compensation near the Kane fracture zone from topography and gravity measurements, I, Spectral analysis approach, *Geophys. J. R. Astron. Soc.*, *68*, 725-750, 1982.

Mahoney, J. J., and K. J. Spencer, Isotopic evidence for the origin of the Manihiki and Ontong Java ocean plateaus, *Earth Planet. Sci. Lett.*, *104*, 196-210, 1991.

Mahoney, J. J., M. Storey, R. A. Duncan, K. J. Spencer, and M. Pringle, Geochemistry and age of the Ontong Java Plateau, in The Mesozoic Pacific: Geology, Tectonics, and Volcanism, Geophys. Monogr. Ser., vol. 77, edited by M. Pringle et al., pp. 233-261, AGU, Washington, D. C., 1993.

Martinod, J., and P. Davy, Periodic instabilities during compression or extension of the lithosphere, 1, Deformation modes from an analytical perturbation method, *J. Geophys. Res.*, *97*, 1999-2014, 1992.

McAdoo, D. C., and D. T. Sandwell, Folding of oceanic lithosphere, *J. Geophys. Res.*, *90*, 8563-8569, 1985.

McKenzie, D., and C. Bowin, The relationship between bathymetry and gravity in the Atlantic Ocean, *J. Geophys. Res.*, *81*, 1903-1915, 1976.

McNutt, M. K., Influence of plate subduction on isostatic compensation in northern California, *Tectonics*, *2*, 399-415, 1983.

McNutt, M. K., Lithospheric flexure and thermal anomalies, *J. Geophys. Res.*, *89*, 11,180-11,194, 1984.

McNutt, M. K., and R. L. Parker, Isostasy in Australia and the evolution of the compensation mechanism, *Science*, *1999*, 773-775, 1978.

McNutt, M. K., D. W. Caress, J. Reynolds, K. A. Jordahl, and R. A. Duncan, Failure of plume theory to explain midplate volcanism in the southern Austral islands, *Nature*, *389*, 479-482, 1997.

Nakanishi, M., K. Tamaki, and K. Kobayashi, Mesozoic magnetic anomaly lineations and seafloor spreading history of the northwestern Pacific, *J. Geophys. Res.*, *94*, 15,437-15,462, 1989.

Neal, C. R., J. J. Mahoney, L. W. Kroenke, R. A. Duncan, and M. G. Petterson, The Ontong Java Plateau, in Large Igneous Provinces, Geophys. Monogr. Ser., vol. 100, edited by J. J. Mahoney and M. F. Coffin, pp.183-216, AGU, Washington, D. C., 1997.

O'Connor, J. M., and R. A. Duncan, Evolution of the Walvis Ridge-Rio Grande Rise hot spot system: Implications for African and South American plate motions over plumes, *J. Geophys. Res.*, *95*, 17,475-17,502, 1990.

Parker, R. L., The rapid calculation of potential anomalies, *Geophys. J. R. Astron. Soc.*, *31*, 447-455, 1973.

Petterson, M. G., C. R. Neal, J. J. Mahoney, L. W. Kroenke, A. D. Saunders, T. L. Babbs, R. A. Duncan, D. Tolia, and B. McGrail, Structure and deformation of north and central Malaita, Solomon Islands: Tectonic implications for the Ontong Java Plateau-Solomon arc collision, and for the fate of oceanic plateaus, *Tectonophysics*, *283*, 1-33, 1997.

Phipps Morgan, J., W. J. Morgan, and E. Price, Hotspot melting generates both hotspot volcanism and a hotspot swell?, *J. Geophys. Res.*, *100*, 8045-8062, 1995.

Richards, M. A., R. A. Duncan, and V. E. Courtillot, Flood basalts and hotspot tracks: Plume heads and tails, *Science*, *246*, 103-107, 1989.

Saltzer, R. L., and E. D. Humphreys, Upper mantle *P* wave velocity structure of the eastern Snake River Plain and its relationship to geodynamic models of the region, *J. Geophys. Res.*, *102*, 11,829-11,841, 1997.

Sandwell, D., and W. H. F. Smith, Marine gravity from Geosat and ERS-1 altimetry, *J. Geophys. Res.*, *102*, 10,039-10,054, 1997.

Sandwell, D. T., and M. L. Renkin, Compensation of swells and plateaus in the northern Pacific: No direct evidence for mantle convection, *J. Geophys. Res.*, *93*, 2775-2783, 1988.

Sandwell, D. T., E. L. Winterer, J. Mammerickx, R. A. Duncan, M. A. Lynch, D. A. Levitt, and C. L. Johnson, Evidence for diffuse extension of the Pacific plate from Pukapuka ridges and cross-grain gravity lineations, *J. Geophys. Res.*, *100*, 15,087-15,099, 1995.

Saunders, A. D., J. G. Fitton, A. C. Kerr, M. J. Norry, and R. W. Kent, "The North Atlantic igneous province", in Large Igneous Provinces, Geophys. Monogr. Ser., vol. 100, edited by J. J. Mahoney and M. F. Coffin, pp. 45-94, AGU, Washington, D. C., 1997.

Stephenson, R., and K. Lambeck, Isostatic response of the lithosphere with in-plane stress: Application to Central Australia, *J. Geophys. Res.*, *90*, 8581-8588, 1985.

Tackley, P. J., and D. J. Stevenson, Volcanism without plumes: Melt-driven instabilities, buoyant residuum and global implications, *Eos Trans. AGU*, *74*(16), Spring Meet. Suppl., 188, 1993.

Tarduno, J. A., W. V. Sliter, L. W. Kroenke, M. Leckie, J. J. Mahoney, R. J. Musgrave, M. Storey, and E. L. Winterer, Rapid formation of Ontong Java Plateau by Aptian mantle plume volcanism, *Science*, *254*, 399-403, 1991.

Tejada, M. L. G., J. J. Mahoney, R. A. Duncan, and M. P. Hawkins, Age and geochemistry of basement and alkalic rocks of Malaita and Santa Isabel, Solomon Islands, southern margin of Ontong Java Plateau, *J. Petrol.*, *37*, 361-394, 1996.

ten Brink, U. S., and T. M. Brocher, Multichannel seismic evidence for a subcrustal intrusive complex under Oahu and a model for Hawaiian volcanism, *J. Geophys. Res.*, *92*, 13,687-13,707, 1987.

Watts, A. B., An analysis of isostasy in the world's oceans, 1, Hawaiian-Emperor seamount chain, *J. Geophys. Res.*, *83*, 5989-6004, 1978.

Watts, A. B., and J. R. Cochran, Gravity anomalies and flexure of the lithosphere along the Hawaiian-Emperor Seamount Chain, *Geophys. J. R. Astron. Soc.*, *38*, 119-141, 1974.

Watts, A. B., J. H. Bodine, and N. M. Ribe, Observations of flexure and the geological evolution of the Pacific Ocean basin, *Nature*, *283*, 532-537, 1980.

Watts, A. B., U. S. ten Brink, P. Buhl, and T. M. Brocher, A multichannel seismic study of lithospheric flexure across the Hawaiian-Emperor seamount chain, *Nature*, *315*, 105-111, 1985.

Weis, D., and F. A. Frey, Role of the Kerguelen plume in generating the eastern Indian Ocean seafloor, *J. Geophys. Res.*, *101*, 13,831-13,849, 1996.

Wessel, P., and L. W. Kroenke, New evidence of a late Neogene change in Pacific Plate absolute motion, *Eos Trans. AGU*, *78*(46), Fall Meet. Suppl., F726, 1997.

Wessel, P., and W. H. F. Smith, New version of the Generic Mapping Tools released, *Eos Trans. AGU*, *76*, 329, 1995.

Winterer, E. L., and M. Nakanishi, Evidence for a plume-augmented, abandoned spreading center on Ontong Java Plateau, *Eos Trans. AGU*, *76*(45), Fall Meet. Suppl., 617, 1995.

Zuber, M. T., Compression of oceanic lithosphere: An analysis of intraplate deformation in the central Indian Basin, *J. Geophys. Res.*, *92*, 4817-4825, 1987.

Zuber, M. T., T. D. Bechtel, and D. W. Forsyth, Effective elastic thicknesses of the lithosphere and mechanisms of isostatic compensation in Australia, *J. Geophys. Res.*, *94*, 9353-9367, 1989.

G. Ito, Department of Geology, One Shields Ave., University of California, Davis, CA 95616. (gito@geology.ucdavis.edu)

A. Taira, Ocean Research Institute, University of Tokyo, 1-15-1 Minamidai, Nakano-ku, Tokyo 164-8639, Japan. (ataira@ori.u-tokyo.ac.jp)

(Received June 10, 1999; revised December 10, 1999; accepted January 26, 2000.)